Development of limb bone laminarity in the domestic pigeon (*Columba livia*) (#46738)

First submission

Guidance from your Editor

Please submit by **28 Mar 2020** for the benefit of the authors (and your $200 publishing discount) .

Structure and Criteria
Please read the 'Structure and Criteria' page for general guidance.

Raw data check
Review the raw data.

Image check
Check that figures and images have not been inappropriately manipulated.

Privacy reminder: If uploading an annotated PDF, remove identifiable information to remain anonymous.

Files

Download and review all files from the materials page.

5 Figure file(s)
3 Table file(s)
8 Other file(s)

Structure your review

The review form is divided into 5 sections. Please consider these when composing your review:

1. **BASIC REPORTING**
2. **EXPERIMENTAL DESIGN**
3. **VALIDITY OF THE FINDINGS**
4. General comments
5. Confidential notes to the editor

You can also annotate this PDF and upload it as part of your review

When ready submit online.

Editorial Criteria

Use these criteria points to structure your review. The full detailed editorial criteria is on your guidance page.

BASIC REPORTING

- Clear, unambiguous, professional English language used throughout.
- Intro & background to show context. Literature well referenced & relevant.
- Structure conforms to PeerJ standards, discipline norm, or improved for clarity.
- Figures are relevant, high quality, well labelled & described.
- Raw data supplied (see PeerJ policy).

EXPERIMENTAL DESIGN

- Original primary research within Scope of the journal.
- Research question well defined, relevant & meaningful. It is stated how the research fills an identified knowledge gap.
- Rigorous investigation performed to a high technical & ethical standard.
- Methods described with sufficient detail & information to replicate.

VALIDITY OF THE FINDINGS

- Impact and novelty not assessed. Negative/inconclusive results accepted. *Meaningful* replication encouraged where rationale & benefit to literature is clearly stated.
- All underlying data have been provided; they are robust, statistically sound, & controlled.
- Speculation is welcome, but should be identified as such.
- Conclusions are well stated, linked to original research question & limited to supporting results.

Standout reviewing tips

The best reviewers use these techniques

Tip	*Example*
Support criticisms with evidence from the text or from other sources	*Smith et al (J of Methodology, 2005, V3, pp 123) have shown that the analysis you use in Lines 241-250 is not the most appropriate for this situation. Please explain why you used this method.*
Give specific suggestions on how to improve the manuscript	*Your introduction needs more detail. I suggest that you improve the description at lines 57- 86 to provide more justification for your study (specifically, you should expand upon the knowledge gap being filled).*
Comment on language and grammar issues	*The English language should be improved to ensure that an international audience can clearly understand your text. Some examples where the language could be improved include lines 23, 77, 121, 128 – the current phrasing makes comprehension difficult.*
Organize by importance of the issues, and number your points	*1. Your most important issue* *2. The next most important item* *3. …* *4. The least important points*
Please provide constructive criticism, and avoid personal opinions	*I thank you for providing the raw data, however your supplemental files need more descriptive metadata identifiers to be useful to future readers. Although your results are compelling, the data analysis should be improved in the following ways: AA, BB, CC*
Comment on strengths (as well as weaknesses) of the manuscript	*I commend the authors for their extensive data set, compiled over many years of detailed fieldwork. In addition, the manuscript is clearly written in professional, unambiguous language. If there is a weakness, it is in the statistical analysis (as I have noted above) which should be improved upon before Acceptance.*

Development of limb bone laminarity in the domestic pigeon (*Columba livia*)

Rylee S McGuire [1], **Raffi M Ourfalian** [1, 2], **Kelly Ezell** [3], **Andrew H Lee** [Corresp. 1, 3, 4]

[1] Arizona College of Osteopathic Medicine, Midwestern University, Glendale, Arizona, United States

[2] Kaiser Permanente Los Angeles Medical Center, Los Angeles, California, United States

[3] Department of Anatomy, College of Graduate Studies, Midwestern University, Glendale, Arizona, United States

[4] College of Veterinary Medicine, Midwestern University, Glendale, Arizona, United States

Corresponding Author: Andrew H Lee
Email address: alee2@midwestern.edu

Background. Birds show adaptations in limb bone shape that are associated with resisting locomotor loads. Whether comparable adaptations occur in the microstructure of avian cortical bone is less clear. One proposed microstructural adaptation is laminar bone in which the proportion of circumferentially-oriented vascular canals (i.e., laminarity) is large. Previous work on adult birds shows elevated laminarity in specific limb elements of some taxa, presumably to resist torsion-induced shear strain during locomotion. However, more recent analyses using improved measurements in adult birds and bats reveal lower laminarity than expected in bones associated with torsional loading. Even so, there may still be support for the resistance hypothesis if laminarity increases with growth and locomotor maturation.

Methods. Here, we tested that hypothesis using a growth series of 17 domestic pigeons (15–563 g). Torsional rigidity and laminarity of limb bones were measured from histological sections sampled from midshaft. Ontogenetic trends in laminarity were assessed using principal components regression.

Results. We found that torsional rigidity of limb bones increases disproportionately with growth, consistent with rapid structural compensation associated with locomotor maturation. However, laminarity decreases with maturity, weakening the hypothesis that elevated laminarity is a flight adaptation at least in the pigeon. These results suggest that the demands of locomotion may drive evolution more strongly at the gross anatomical level rather than at the histological level.

Development of limb bone laminarity in the domestic pigeon (*Columba livia*)

Rylee S. McGuire[1], Raffi M. Ourfalian[1,*], Kelly Ezell[2], Andrew H. Lee[1,2]

[1] Arizona College of Osteopathic Medicine, Midwestern University, Glendale, AZ, USA
[2] Department of Anatomy, College of Graduate Studies, Midwestern University, Glendale, AZ, USA

[*]Current address
Kaiser Permanente Los Angeles Medical Center, Los Angeles, CA, USA

Corresponding Author:
Andrew H. Lee[1]
19555 N 59th Avenue, Glendale, AZ, 85308, USA
Email address: alee712@gmail.com

Abstract

Background. Birds show adaptations in limb bone shape that are associated with resisting locomotor loads. Whether comparable adaptations occur in the microstructure of avian cortical bone is less clear. One proposed microstructural adaptation is laminar bone in which the proportion of circumferentially-oriented vascular canals (i.e., laminarity) is large. Previous work on adult birds shows elevated laminarity in specific limb elements of some taxa, presumably to resist torsion-induced shear strain during locomotion. However, more recent analyses using improved measurements in adult birds and bats reveal lower laminarity than expected in bones associated with torsional loading. Even so, there may still be support for the resistance hypothesis if laminarity increases with growth and locomotor maturation.

Methods. Here, we tested that hypothesis using a growth series of 17 domestic pigeons (15–563 g). Torsional rigidity and laminarity of limb bones were measured from histological sections sampled from midshaft. Ontogenetic trends in laminarity were assessed using principal components regression.

Results. We found that torsional rigidity of limb bones increases disproportionately with growth, consistent with rapid structural compensation associated with locomotor maturation. However, laminarity decreases with maturity, weakening the hypothesis that elevated laminarity is a flight adaptation at least in the pigeon. These results suggest that the demands of locomotion may drive evolution more strongly at the gross anatomical level rather than at the histological level.

Introduction

Laminar bone is a form of fibrolamellar bony tissue in which the primary vascular canal network is organized into concentric interconnected layers (Francillon-Vieillot et al., 1990). It is dominated by circumferential vascular canals (Currey, 1960; Francillon-Vieillot et al., 1990; de Ricqlès et al., 1991; de Margerie, 2002; de Boef & Larsson, 2007; Huttenlocker, Woodward & Hall, 2013), which have elongated profiles in transverse view that run approximately parallel to the periosteal surface (Fig. 1). The proportion of laminar bone [laminarity(de Margerie, 2002)] in many adult avian species appears elevated in specific limb bones such the humerus, ulna, femur, and tibiotarsus (de Margerie et al., 2005). Theoretical modeling suggests that these limb bones experience locomotor-induced torsion (i.e., by flapping in the humerus and ulna and by walking in the femur and tibiotarsus) (Pennycuick, 1967). Indeed, *in vivo* bone strain measurements confirm that torsional loading is substantial in the ulna of grounded but flapping turkeys (Lanyon & Rubin, 1984) and is dominant in the humerus of flying pigeons (Biewener & Dial, 1995). In addition, while walking, chickens and emus generate large torsional loads occur in the femur and tibiotarsus (Biewener, Swartz & Bertram, 1986; Carrano & Biewener, 1999; Main & Biewener, 2007). If these loading patterns are stereotypical across birds, then the elevated laminarity observed in humeri, ulnae, femora, and tibiotarsi of many avian species may be a general feature of limb bones loaded habitually in torsion (de Margerie et al., 2005).

A purely biomechanical explanation for laminarity, however, remains problematic. Contrary to histological predictions, the only two species with detailed measurements of flight-induced torsion [*Columba livia* (Biewener & Dial, 1995) and *Pteropus poliocephalus* (Swartz, Bennett & Carrier, 1992)] actually have negligible to low laminarity in the adult humerus (Bennett & Forwood, 2010; Lee & Simons, 2015; Pratt et al., 2018). Furthermore, the small amount of laminar bone that is found in the adult pigeon humerus is not localized to the

superficial cortex of the humerus, where maximum flight-induced torsional and bending strains are predicted (Pennycuick, 1967; Carter & Spengler, 1978; Craig, 2000). Instead, it occurs in the deep cortex, presumably remnants from earlier juvenile development. Therefore, further sampling across the development of the pigeon is needed to clarify the extent of laminar bone in juveniles.

Postnatal development in the pigeon is altricial (Starck & Ricklefs, 1998). Juveniles are flightless and nest-bound for most of the postnatal growth period (Vriends & Erskine, 2005; Coles, 2007; Liang et al., 2018). Only when nearly full-grown do they become powerful fliers (Tobalske & Dial, 1996). Thus, the pigeon is ideal to examine rapid structural compensation in the limb skeleton during locomotor transition. Skeletal compensation occurs in the altricial-developing wings of the California gull (Carrier & Leon, 1990) and mallard (Dial & Carrier, 2012), so we expect it in both forelimb and hindlimb of the developing pigeon. Specifically, polar section modulus, which is a standard proxy for torsional rigidity at midshaft (Ruff, 2002; Young, Fernández & Fleagle, 2010; Ruff et al., 2013), should scale with positive ontogenetic allometry. Furthermore, if laminarity is a reflection of locomotor-induced torsion (de Margerie et al., 2005), then it should increase dramatically with skeletal (and locomotor) maturity.

Materials & Methods

Sampling and histology

We acquired salvaged and donated carcasses of 17 homing pigeons (Stromberg's Chicks & Game Birds Unlimited; Pine River, Minnesota, USA). The sample comprises a postnatal growth series of known mass (15 – 563 g) (Table S1). Although the age range of the sample is 0–9 weeks, the precise age of death for most individuals was not recorded. The right fore- and hindlimb of each individual was dissected to reveal the humerus, radius, ulna, femur, and

tibiotarsus (Fig. 2A). The length of each element was measured (Tables S2–S6), and a 1-cm mid-diaphyseal block from each bone was excised using a rotary tool (Dremel 4000; Dremel, Mt. Prospect, Illinois, USA). We followed an established protocol for preparing plastic-embedded undecalcified bone (Lee & Simons, 2015). Two transverse 700-µm wafers were cut from each specimen at mid-diaphysis using a precision saw (Isomet 1000; Buehler, Lake Bluff, Illinois, USA). The wafers were mounted (Gorilla Epoxy; Gorilla Glue Inc., Cincinnati, Ohio, USA) to frosted glass slides and manually ground (Metaserv 250; Buehler, Lake Bluff, Illinois, USA) to 100 ± 10 µm.

Imaging

Sections were acid-etched and stained with toluidine blue (Eurell & Sterchi, 1994) to improve contrast of in-plane primary vascular canals (Fig. 2B). The stain also highlights secondary osteons (specifically cement lines) and their (Haversian) canals, which are traditionally excluded from measurements of laminarity (de Margerie, 2002). Whole section images pre- and post-staining were captured with a motorized upright microscope (Ni-U; Nikon, Tokyo, Japan) with a strain-free objective (10× Plan Fluor: numerical aperture of 0.3, resolvable size ≈1 µm). Once imaging was completed, each section was mounted (Permount; Fisher Scientific, Hampton, New Hampshire, USA) with a glass coverslip (#1; Fisher Scientific, Hampton, New Hampshire, USA) for preservation.

Bone profiles

A bone profile was prepared from each montage using Photoshop (CS5; Adobe, San Jose, California, USA). Montages were sharpened with the “Unsharp Mask” filter set at 5 px and are

high resolution (2.1 μm per pixel). The area bounded between the periosteal and endosteal surfaces was filled with white to represent bone. The surrounding non-bone area as well as in-plane vascular canals and resorption spaces were filled with black. Bone profiles were exported to ImageJ (1.51d; National Institutes of Health, Bethesda, Maryland, USA) for further analysis. We measured the periosteal circumference and vascular porosity (areal ratio of in-plane vascular canals to total cortical area) of each bone profile (Tables S2–S6). Montages and bone profiles are freely accessible as interactive digital slides at the Paleohistology Repository (Lee & O'Connor, 2013).

Ontogenetic scaling of polar section modulus

We used BoneJ v1.4.1 (Doube et al., 2010) to estimate the polar section modulus (Z_p), which is a proxy of torsional rigidity and average bone bending rigidity (Ruff, 2002), for each bone (Tables S2–S6). This proxy is appropriate when the cross section of a long bone is nearly circular (Craig, 2000). To test the suitability of this proxy to each cross section, we used BoneJ to calculate I_{min}/I_{max}, which is equal to 1.0 in a circular cross section. Values for the bone sections range from 1.03 to 1.80 (Tables S2–S6). When compared to a reference figure (Daegling, 2002), the values of I_{min}/I_{max} in our sample suggest errors in torsional rigidity less than 6.7%. Therefore, we find no major problem in using this proxy.

Using R (R Core Team, 2019), linear regression was performed separately for each element between log10-transformed Z_p and the log10-transformed product of body mass and bone length. The coefficients of the regression analysis are presented in Table 1 and allometric scaling was inferred if the 95% confidence interval on slopes excluded the value of 0.75 (isometry) (Young, Fernández & Fleagle, 2010).

Laminarity index. We classified each vascular canal into one of four discrete categories of orientation (longitudinal, radial, oblique, and circumferential). Although, the laminarity index (LI) was originally defined by de Margerie (2002) as the proportionate area of circumferential canals relative to the total area of vascular canals, we used a subsequent re-definition in which LI is the number of circumferential canals divided by the total number of canals (Simons & O'Connor, 2012; Legendre et al., 2014; Lee & Simons, 2015). As such LI is a proportion and ranges from 0 (absence of circumferential canals) to 1 (ubiquity of circumferential canals).

We adopted a recently published method to quantify LI (Lee & Simons, 2015). Instead of counting every canal in an image of a bone section, we systematically sampled approximately 50% of the canals in a given section. The image of each section was divided into octants using Photoshop (Fig. 2B), and the four octants representing cardinal anatomical positions (i.e., cranial, caudal, dorsal, and ventral for the wing elements; cranial, caudal, medial, and lateral for the hindlimb elements) were extracted for analysis.

Canal orientation is measured relative to the local tangent to the periosteal surface. That surface, however, is curved in most bone cortices (Fig. 2C). Consequently, the local tangent varies across a curved cortex and requires repeated referencing to measure canal orientation. To increase throughput and minimize error, we straightened the curvature of each octant using the "Straighten" function in ImageJ. Once straightened, the periosteal surface is parallel with the horizontal, thereby establishing a constant reference line (Fig. 2D). To assess the amount of distortion caused by straightening, we placed circular clock-shaped profiles with the clock hands placed at known angles in the original curved octants. We then re-measured profiles and angles after straightening each octant to assess the extent of image deformation on canal orientation.

Overall, the median deviation of test angles from original values is 1.15°, and the median aspect ratio of circular profiles is 1.05. At least in this study, canal orientation in straightened octants appears accurate.

We adopted the method by de Boef and Larsson (2007) to approximate the sectional profile of each primary vascular canal with a best-fitting ellipse using ImageJ. For each ellipse, the aspect ratio and orientation of the major axis relative to the periosteal reference line were measured. To relate these measurements to canal orientation, we followed criteria proposed by de Margerie (2002): (1) longitudinal canals have an aspect ratio of less than 3; (2) circumferential canals have major axes oriented 0° ± 22.5° relative to the nearest tangent line drawn at the periosteal surface; (3) radial canals have major axes oriented 90°± 22.5° relative to the nearest tangent line drawn at the periosteal surface; and (4) all remaining canals are oblique (Fig. 2E). Any canal that branches was divided at the node, and the orientation of each subdivided canal was estimated using the methodology as described above.

The ellipse-fitting method is appropriate as long as canals are generally cylindrical. They tend to be in cortical bone (Cooper et al., 2003, 2011; Pratt & Cooper, 2017), which ranges in vascular porosity from 0 – 30% (Carter & Spengler, 1978; Zioupos, Cook & Hutchinson, 2008). MicroCT inspection suggests this assumption is reasonable for avian cortical bone (Fig. 1). However, in cancellous bone (Carter & Spengler, 1978; Zioupos, Cook & Hutchinson, 2008) with vascular porosity greater than 30%, canals are too irregular to approximate with the ellipse-fitting method. Consequently, we measured canal orientation only in bone sections with porosity less than or equal to 30% (Tables S2–S6), and laminarity for youngest specimens (MWU263, MWU 261, MWU 260, and MWU 267) was not measured.

Robust principal component analysis and beta regression

In this study, we had to address the issue of multicollinearity among our explanatory variables: mass, bone length, and *Zp*. Principal component analysis (PCA) enables the formation of new, uncorrelated predictors (principal components) through linear combinations of the original variables. As such, we were able to resolve the issue of multicollinearity while still being able to assess the effect of each variable (Fekedulegn et al., 2002). PCA, however, is known to be highly sensitive to non-normal data. Therefore, we used robust PCA, which is appropriate for skewed data (Hubert, Rousseeuw & Verdonck, 2009), as implemented by the R package "rospca" (Reynkens, 2018). We standardized mass, bone length, and *Zp* by median and median absolute deviation with the function "RobScale" (Signorell, 2019) in R. Robust PCA was performed separately for each element (Table 2).

We used regression analysis to relate the minimum number of principal components (PCs) that account for at least 95% of the variation in the original variables with laminarity. However, laminarity index (LI) values do not satisfy assumptions required of traditional linear regression because they are not normally distributed and are bounded between 0 and 1. To overcome these problems, we used beta regression model with a logit link function to connect the mean LI to the predictor(s) as follows:

$$\mu_{logit(\mathrm{LI})} = \beta_0 + \beta_i PC_i + \ldots + \beta_k PC_k,\ i = 1, \ldots, k$$

where $\mu_{logit(\mathrm{LI})}$ is the logit link function for the mean of LI, $PC_i, \ldots, PC_k$ are the principal components, β_0 is the intercept, $\beta_i, \ldots, \beta_k$ are coefficients corresponding to each principal component, and k is the number of principal components (Ferrari & Cribari-Neto, 2004). Analyses were performed with the R package "gamlss" (Rigby & Stasinopoulos, 2005).

Results

Histological description

At mid-diaphysis, the limb bones of the pigeon become increasingly compact with growth (Tables S2–S6). In very young individuals ranging from 0–2 weeks, bone walls are relatively thick and largely cancellous (porosity > 30%) with irregular vascular spaces. That cancellous structure is consistent with rapidly-growing juvenile bone as seen in other avian species (de Margerie et al., 2004). Older individuals show compact bone with vascular canals. For each bone, peak laminarity (i.e., proportion of circumferentially oriented canals) occurs in juveniles aged 2–4 weeks (Figs. 2 and 3). As individuals mature (4–9 weeks of age), they deposit new bony tissue with poor vascularization along the superficial half to third of the cortical wall (Fig. 3A–J). Although the remaining deep portion is highly vascularized, canals are predominantly longitudinal (Fig. 3A–J).

Zp scaling analysis

The polar section modulus (Z_p) of the humerus, radius, ulna, femur, and tibiotarsus increases with growth (Tables S2–S6). When scaled to the log10-transformed product of body mass and bone length, log10-transformed *Zp* shows positive allometry for all five sampled elements (Fig. 4). The allometric slope of the tibiotarsus is slightly (but not significantly) shallower than the slopes of the other elements, in part reflecting the relatively large size of the tibiotarsus at hatch (Table 1).

Robust principal component analysis

Robust principal component analysis is generally consistent across the five limb elements (Table 2). PC1 captures at least 95% of the variance in the original predictors: 98% for the humerus,

95% for the radius, 97% for the ulna, 98% for the femur, and 96% for the tibiotarsus. We ignored the residual variance (approximately 2–5%) that is absorbed by PC2 and PC3, thereby reducing data dimensionality from three components to one. Mass, Z_p (torsional rigidity), and bone length each have positive loadings on PC1. In the humerus, ulna, and femur, length and Z_p share dominance on PC1 (Table 2). However in the radius and tibiotarsus, length alone dominates PC1 (Table 2). Nevertheless, the loadings are consistent with PC1 representing an ontogenetic axis. Small PC1 scores are associated with juvenile features (small mass with short bones that are relatively compliant to torsion), whereas large PC1 scores are associated with adult features (large mass with long bones that are relatively rigid to torsion).

Beta regression

Although each element shows a significant negative correlation between laminarity index (LI) and PC1 (Table 3), two groups are apparent. The first group consists of humerus, ulna, and femur. This group is characterized by models with relatively strong goodness-of-fit (pseudo-R^2 exceeds 0.70), relatively positive intercept, and steep negative slope. In contrast to the first group, the second group consists of radius and tibiotarsus. It features models with relatively weak goodness-of-fit (pseudo-$R^2 < 0.55$), relatively negative intercept, and shallow negative slope. Put together these results demonstrate that laminarity decreases with ontogeny and that laminarity in the radius and tibiotarsus may be influenced by additional factors (Fig. 5).

We converted the PC1 coefficient into standardized coefficients of the original predictors (mass, length, and Z_p). The relative effects of bone length and Z_p dominate in the humerus, ulna, and femur, whereas in the radius and tibiotarsus, the relative effect of bone length dominates. Nevertheless in each element, we found negative correlations between the original predictors and

laminarity (Table 3). Contrary to expectations, these results in the pigeon suggest that as bones grow increasingly rigid to torsion, their laminarity decreases.

Discussion

Maturation of pigeon limb bones is synchronized and typical of altricial development. Each of the five limb elements analyzed shows positive allometry in polar section modulus (Z_p) (Fig. 4; Table 1). Compared to juveniles, adults have limb bones that are disproportionately rigid to torsion, consistent with relatively late locomotor maturation. Onset of walking and coordinated flapping of wings occurs 14–21 days post-hatch, and locomotor maturation is complete around 28–42 days post-hatch (Levi, 1962; Janiga & Kocian, 1985; Johnston & Janiga, 1995; Vriends & Erskine, 2005; Liang et al., 2018). Our interpretation in the pigeon wing is consistent with previous work showing strong positive allometry in wing bones of the California gull, black tern, and mallard, each of which are unable to fly until nearly full-grown. Unlike the pigeon, those birds begin walking shortly after hatch. As such, juveniles benefit from relatively robust skeletal proportions (negative allometry), presumably to keep immature tissues within safety margins during locomotion. Put together, our results support previous interpretations that cross-sectional bone geometry is a useful proxy for habitual loading and locomotor maturity (Swartz, Bennett & Carrier, 1992; Main & Biewener, 2007; Habib & Ruff, 2008; Young, Fernández & Fleagle, 2010). Moreover, the growth of torsional rigidity in wing bones is consistent with rapid structural compensation related to the demands of flight (Carrier & Leon, 1990; Bennett, 2008; Dial & Carrier, 2012).

Contrary to expectations, the relatively rigid bones of adult pigeons have low laminarity (Figs. 3 and 5). This result differs from a recent study of 14 adult pigeons in which laminarity was reported as “high” (Skedros & Doutré, 2019). However, that study neither stained thick

undecalcified sections to clearly define boundaries of in-plane canals nor quantified canal orientation. Therefore, we cannot exclude that possibility that the reported "high laminarity" is overestimated.

In other avian taxa, low laminarity is attributed to reduced torsional loading such as in specialized soaring birds with long narrow wings that presumably are not suited for frequent flapping (de Margerie et al., 2005; Simons & O'Connor, 2012). Clearly, that explanation does not apply to the pigeon, which is a generalist flier (Berg & Biewener, 2010) with *in vivo* strain data from the humerus indicating considerable torsion during flapping (Biewener & Dial, 1995). Although strain data are not available for the remaining bones that we sampled in the pigeon, data from other avian species indicate similar torsional loading in the ulna of turkey and the femur of chicken during grounded flapping and walking, respectively (Lanyon & Rubin, 1984; Carrano & Biewener, 1999). These data suggest a systemic mismatch between laminarity and loading in the adult pigeon. They also address criticism regarding a similar mismatch in bats (Lee & Simons, 2015; Pratt et al., 2018), whose bones are simply not vascularized enough to be laminar. Here we show that even when richly vascularized as in the pigeon, torsionally-loaded bone is not necessarily more laminar.

Peak laminarity in pigeons occurs in nest-bound juveniles but is transient (Figs. 3 and 5). Juveniles begin to exercise their limbs a few weeks after hatching (Levi, 1962; Janiga & Kocian, 1985; Johnston & Janiga, 1995; Vriends & Erskine, 2005; Liang et al., 2018), so elevated laminarity in their bones, especially in the humerus, ulna, and femur, suggests a response to torsional loading. Contrary to expectations, elevated laminarity is not maintained in growing juveniles as they intensify limb movements shortly before fledging. Instead, laminarity decreases as cross-sectional rigidity increases (Table 3). These results in the pigeon further weaken the

hypothesis that laminar bone develops to improve torsional rigidity. Future directions include assessing material properties, which may contribute to bone rigidity in pigeons and birds more broadly.

Currently, comparisons to other avian taxa are limited because the development of laminarity has only been quantified in the pigeon and emu. Even so, there is evidence that development of laminarity varies across birds. In the pigeon, laminarity and ontogeny are inversely correlated (Table 3). However in the emu, their relationship is more complex. Laminarity is highly variable and independent of ontogeny in the diminutive wing, presumably reflecting relaxed selection from flightlessness, whereas it is positively correlated with ontogeny in the hindlimb (Kuehn et al., 2019). Even so, among the sampled ontogenetic parameters (body mass, postnatal age, growth rate, and caudal shear strain), shear strain has the weakest effect on laminarity based on standardized regression coefficients. Furthermore, residual variation in shear strain not accounted for by ontogeny forms a "loading axis", but it is not a significant predictor of laminarity. Put together, the results from pigeons and emus suggest that torsion-induced shear strain might have a minor effect on laminarity, but ontogenetic effects clearly dominate in bones selected for locomotion.

The developmental approach used by the current study may inform how loading affects other histological features such as collagen fiber orientation. In adult birds, collagen fibers with oblique-to-transverse orientation are especially abundant in bones shaped to resist torsion (de Margerie et al., 2005). Those features evolved independently in adult birds and at least one species of fruit bat (Skedros & Doutré, 2019) suggesting that they may be fundamental adaptations of vertebrate flapping flight. If so, we expect collagen fiber obliquity and torsional rigidity of wing bones to increase with locomotor maturity. Preliminary evidence suggests that

the predicted trend occurs in the ulna of growing turkey (Skedros et al., 2003). Future investigations should apply the developmental approach across a broader phylogenetic sample.

Conclusions

Limb bones that experience locomotor-induced torsion do not necessarily develop elevated laminarity. On the contrary, limb bone laminarity decreases systemically with maturity at least in the pigeon. This developmental pattern differs from a recent report in growing emus, suggesting that factors other than load resistance influence laminarity. At present, the hypothesis that adaptation to locomotor-induced torsion involves elevated bone laminarity is not supported. There is strong evidence, however, that limb bone geometry adapts to loading. Unlike laminarity, bone geometry develops disproportionate rigidity to torsion as juveniles mature into adults. This result is consistent with previous findings and suggests that the demands of locomotion may drive evolution more strongly at the gross anatomical level rather than at the histological level.

Acknowledgements

We thank Stromberg's Chicks and Gamebirds for access to their salvaged pigeons. Erin Simons provided access to shared lab supplies and equipment. Ravi Bhadriraju, who at the time was a research volunteer and federal work study student, prepared slides of the femur and tibiotarsus. Volumetric renders in Figures 1 and 2 were generated from microCT scanning performed by Baker Hughes Inspection Technologies and Nikon Metrology as well as from CT scanning performed by Sasha Willis at Midwestern University's Companion Animal Clinic. This is Arizona Research Collection for Integrative Vertebrate Education and Study (ARCIVES) contribution no. XXXX.

References

Bennett MB. 2008. Post-hatching growth and development of the pectoral and pelvic limbs in the black noddy, *Anous minutus*. *Comparative Biochemistry and Physiology Part A: Molecular & Integrative Physiology* 150:159–168. DOI: 10.1016/j.cbpa.2006.06.011.

Bennett MB, Forwood MR. 2010. Histomorphometric changes in the wing bones of the fruit bat, *Pteropus poliocephalus*, (Megachiroptera: Pteropidae [*sic* Pteropodidae]) in relation to increased bone strain and the failure of a good (?) hypothesis. *Australian Zoologist* 35:341–348.

Berg AM, Biewener AA. 2010. Wing and body kinematics of takeoff and landing flight in the pigeon (*Columba livia*). *The Journal of Experimental Biology* 213:1651. DOI: 10.1242/jeb.038109.

Biewener AA, Dial KP. 1995. In vivo strain in the humerus of pigeons (*Columba livia*). *Journal of Morphology* 225:61–75. DOI: 10.1002/jmor.1052250106.

Biewener AA, Swartz SM, Bertram JEA. 1986. Bone modeling during growth: dynamic strain equilibrium in the chick tibiotarsus. *Calcified Tissue International* 39:390–395.

de Boef M, Larsson HCE. 2007. Bone microstructure: quantifying bone vascular orientation. *Canadian Journal of Zoology* 85:63–70.

Carrano MT, Biewener AA. 1999. Experimental alteration of limb posture in the chicken (*Gallus gallus*) and its bearing on the use of birds as analogs for dinosaur locomotion. *Journal of Morphology* 240:237–249.

Carrier D, Leon LR. 1990. Skeletal growth and function in the California gull (*Larus californicus*). *Journal of Zoology* 222:375–389.

Carter DR, Spengler DM. 1978. Mechanical properties and composition of cortical bone. *Clinical Orthopaedics and Related Research* 135:192–217.

Coles BH. 2007. Appendix 9: Incubation and fledging periods of selected birds. In: *Essentials of Avian Medicine and Surgery*. Blackwell Publishing Ltd, 355–356.

Cooper DML, Erickson B, Peele AG, Hannah K, Thomas CDL, Clement JG. 2011. Visualization of 3D osteon morphology by synchrotron radiation micro-CT. *Journal of Anatomy* 219:481–489. DOI: 10.1111/j.1469-7580.2011.01398.x.

Cooper D, Turinsky A, Sensen C, Hallgrimsson B. 2003. Quantitative 3D analysis of the canal network in cortical bone by micro computed tomography. *The Anatomical Record Part B: The New Anatomist* 274:169–179.

Craig RR Jr. 2000. *Mechanics of Materials*. New York: John Wiley & Sons, Inc.

Currey JD. 1960. Differences in the blood-supply of bone of different histological types. *Quarterly Journal of Microscopical Sciences* 101:351–370.

Daegling DJ. 2002. Estimation of torsional rigidity in primate long bones. *Journal of Human Evolution* 43:229–239. DOI: 10.1006/jhev.2002.0574.

Dial TR, Carrier DR. 2012. Precocial hindlimbs and altricial forelimbs: partitioning ontogenetic strategies in mallards (*Anas platyrhynchos*). *The Journal of Experimental Biology* 215:3703–3710. DOI: 10.1242/jeb.057380.

Doube M, Kłosowski MM, Arganda-Carreras I, Cordelières FP, Dougherty RP, Jackson JS, Schmid B, Hutchinson JR, Shefelbine SJ. 2010. BoneJ: Free and extensible bone image analysis in ImageJ. *Bone* 47:1076–1079. DOI: 10.1016/j.bone.2010.08.023.

Eurell JAC, Sterchi DL. 1994. Microwaveable toluidine blue stain for surface staining of undecalcified bone sections. *Journal of Histotechnology* 17:357–359. DOI: 10.1179/his.1994.17.4.357.

Fekedulegn BD, Colbert JJ, Hicks Jr. RR, Schuckers ME. 2002. *Coping with multicollinearity: an example on application of principal components regression in dendroecology*. Newtown Square, Pennsylvania: U.S. Department of Agriculture, Forest Service, Northeastern Research Station.

Ferrari S, Cribari-Neto F. 2004. Beta regression for modelling rates and proportions. *Journal of Applied Statistics* 31:799–815. DOI: 10.1080/0266476042000214501.

Francillon-Vieillot H, de Buffrénil V, Castanet J, Geraudie J, Meunier FJ, Sire JY, Zylberberg L, de Ricqlès AJ. 1990. Microstructure and mineralization of vertebrate skeletal tissues. In: Carter JG ed. *Skeletal Biomineralization: Patterns, Processes and Evolutionary Trends*. New York: Van Nostrand Reinhold, 471–548.

Habib MB, Ruff CB. 2008. The effects of locomotion on the structural characteristics of avian limb bones. *Zoological Journal of the Linnean Society* 153:601–624.

Hubert M, Rousseeuw P, Verdonck T. 2009. Robust PCA for skewed data and its outlier map. *Computational Statistics & Data Analysis* 53:2264–2274. DOI: 10.1016/j.csda.2008.05.027.

Huttenlocker AK, Woodward HN, Hall BK. 2013. The biology of bone. In: Padian K, Lamm E-T eds. *Bone Histology of Fossil Tetrapods: Advancing Methods, Analysis, and Interpretation*. Berkeley, California: University of California Press, 13–34.

Janiga M, Kocian L. 1985. The knowledge of postnatal development of the feral pigeon (*Columba livia* f. *domestica*) in Bratislava. *Biológia (Bratislava)* 40:189–197.

Johnston RF, Janiga M. 1995. *Feral Pigeons*. New York: Oxford University Press.

Kuehn AL, Lee AH, Main RP, Simons ELR. 2019. The effects of growth rate and biomechanical loading on bone laminarity within the emu skeleton. *PeerJ* 7:e7616. DOI: 10.7717/peerj.7616.

Lanyon LE, Rubin CT. 1984. Static vs. dynamic loads as an influence on bone remodeling. *Journal of Biomechanics* 17:897–905.

Lee AH, O'Connor PM. 2013. Bone histology confirms determinate growth and small body size in the noasaurid theropod *Masiakasaurus knopfleri*. *Journal of Vertebrate Paleontology* 33:865–876. DOI: 10.1080/02724634.2013.743898.

Lee AH, Simons ELR. 2015. Wing bone laminarity is not an adaptation for torsional resistance in bats. *PeerJ* 3:e823. DOI: 10.7717/peerj.823.

Legendre LJ, Bourdon E, Scofield RP, Tennyson AJD, Lamrous H, de Ricqlès A, Cubo J. 2014. Bone histology, phylogeny, and palaeognathous birds (Aves: Palaeognathae). *Biological Journal of the Linnean Society* 112:688–700. DOI: 10.1111/bij.12312.

Levi WM. 1962. *The Pigeon*. Sumter, SC: Levi Publishing.

Liang X, Yu J, Wang H, Zhang Z. 2018. Post-hatching growth of the pectoralis muscle in pigeon and its functional implications. *The Anatomical Record* 301:1564–1569. DOI: 10.1002/ar.23850.

Main RP, Biewener AA. 2007. Skeletal strain patterns and growth in the emu hindlimb during ontogeny. *Journal of Experimental Biology* 210:2676.

de Margerie E. 2002. Laminar bone as an adaptation to torsional loads in flapping flight. *Journal of Anatomy* 201:521–526. DOI: 10.1046/j.1469-7580.2002.00118.x.

de Margerie E, Robin J-P, Verrier D, Cubo J, Groscolas R, Castanet J. 2004. Assessing a relationship between bone microstructure and growth rate: a fluorescent labelling study in

the king penguin chick (*Aptenodytes patagonicus*). *Journal of Experimental Biology* 207:869–879.

de Margerie E, Sanchez S, Cubo J, Castanet J. 2005. Torsional resistance as a principal component of the structural design of long bones: comparative multivariate evidence in birds. *Anatomical Record* 282A:49–66. DOI: 10.1002/ar.a.20141.

Pennycuick CT. 1967. The strength of the pigeon's wing bones in relation to their function. *Journal of Experimental Biology* 46:219–233.

Pratt IV, Cooper DML. 2017. A method for measuring the three-dimensional orientation of cortical canals with implications for comparative analysis of bone microstructure in vertebrates. *Micron* 92:32–38. DOI: 10.1016/j.micron.2016.10.006.

Pratt IV, Johnston JD, Walker E, Cooper DML. 2018. Interpreting the three-dimensional orientation of vascular canals and cross-sectional geometry of cortical bone in birds and bats. *Journal of Anatomy* 232:931–942. DOI: 10.1111/joa.12803.

R Core Team. 2019. *R: A language and environment for statistical computing*. Vienna, Austria: R Foundation for Statistical Computing.

Reynkens T. 2018. *rospca: Robust Sparse PCA using the ROSPCA Algorithm*.

de Ricqlès AJ, Meunier FJ, Castanet J, Francillon-Vieillot H. 1991. Comparative microstructure of bone. In: Hall BK ed. *Bone, Volume 3: Bone Matrix and Bone Specific Products*. Boston: CRC Press, 1–78.

Rigby RA, Stasinopoulos DM. 2005. Generalized additive models for location, scale and shape. *Applied Statistics* 54:507–554.

Ruff CB. 2002. Long bone articular and diaphyseal structure in old world monkeys and apes. I: Locomotor effects. *American Journal of Physical Anthropology* 119:305–342. DOI: 10.1002/ajpa.10117.

Ruff CB, Burgess ML, Bromage TG, Mudakikwa A, McFarlin SC. 2013. Ontogenetic changes in limb bone structural proportions in mountain gorillas (*Gorilla beringei beringei*). *Journal of Human Evolution* 65:693–703.

Simons ELR, O'Connor PM. 2012. Bone laminarity in the avian forelimb skeleton and its relationship to flight mode: testing functional interpretations. *The Anatomical Record* 295:386–396. DOI: 10.1002/ar.22402.

Skedros JG, Doutré MS. 2019. Collagen fiber orientation pattern, osteon morphology and distribution, and presence of laminar histology do not distinguish torsion from bending in bat and pigeon wing bones. *Journal of Anatomy* 234:748–763. DOI: 10.1111/joa.12981.

Skedros JG, Hunt KJ, Hughes PE, Winet H. 2003. Ontogenetic and regional morphological variations in the turkey ulna diaphysis: implications for functional adaptation of cortical bone. *Anatomical Record* 273A:609–629.

Starck JM, Ricklefs RE. 1998. Patterns of development: the altricial-precocial spectrum. In: *Avian growth and development. Evolution within the altricial-precocial spectrum*. New York: Oxford University Press, 3–30.

Swartz SM, Bennett MB, Carrier DR. 1992. Wing bone stresses in free flying bats and the evolution of skeletal design for flight. *Nature* 359:726–729. DOI: 10.1038/359726a0.

Tobalske B, Dial K. 1996. Flight kinematics of black-billed magpies and pigeons over a wide range of speeds. *Journal of Experimental Biology* 199:263–280.

Vriends MM, Erskine TE. 2005. *Pigeons*. New York: Barron's Educational Series, Inc.

Young JW, Fernández D, Fleagle JG. 2010. Ontogeny of long bone geometry in capuchin monkeys (*Cebus albifrons* and *Cebus paella*): implications for locomotor development and life history. *Biology Letters* 6:197–200. DOI: 10.1098/rsbl.2009.0773.

Zioupos P, Cook RB, Hutchinson JR. 2008. Some basic relationships between density values in cancellous and cortical bone. *Journal of Biomechanics* 41:1961–1968. DOI: 10.1016/j.jbiomech.2008.03.025.

Figure 1

Vascular canals in avian cortical bone are networked but generally cylindrical.

(**A**) Whole humerus scanned with microCT at 8-µm voxel resolution reveals thin cortical wall at mid-diaphysis. (**B**) Virtual transverse section of a cortical strip sampled from mid-diaphysis at 4-µm voxel resolution looks comparable to a traditionally prepared histological section. Volumetric visualization in transverse (**D**) and tangential planes (**D,E**) reveal cylindrical shape of canals. Whole bone and cortical strip were scanned using a GE phoenix v|tome|x and Nikon XT H 225, respectively. Segmentation and rendering performed with Avizo (9.0.1, FEI).

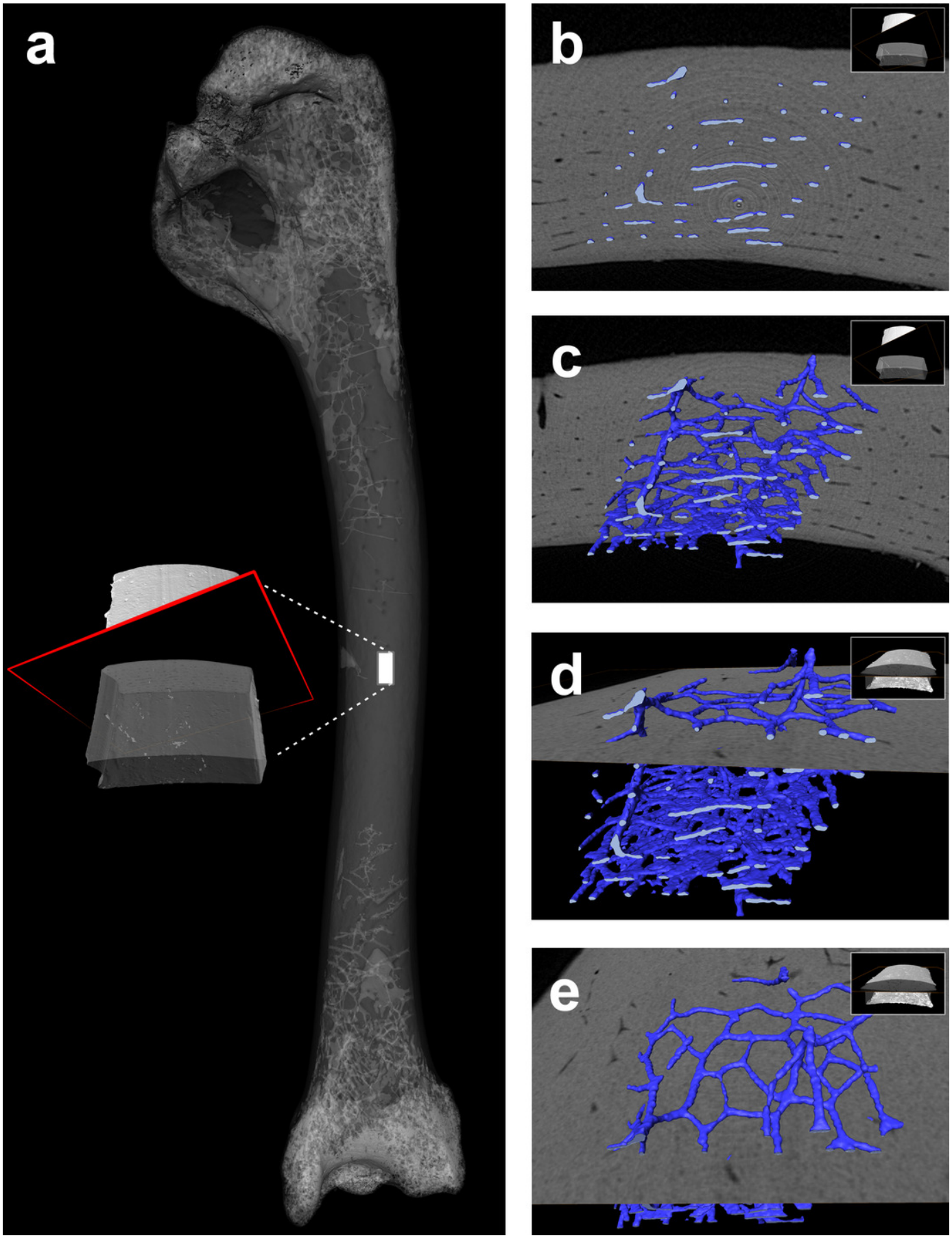
a
b
c
d
e

Figure 2

Bone profile preparation for evaluation of laminarity index.

(**A**) Mid-diaphyseal cross-sections were taken from the five listed bone elements harvested from a growth series of 17 pigeons (left-sided elements imaged using a Siemens SOMATOM Perspective CT scanner only for illustrative purposes). (**B**) Each section was divided into four octants representing cardinal anatomical positions (i.e., cranial, caudal, dorsal, and ventral for the wing elements; cranial, caudal, medial, and lateral for the hindlimb elements). Octant curvature (**C**) was straightened (**D**) using ImageJ. (**E**) Canals were fit with ellipses and classified based on orientation relative to the horizontal periosteal surface.

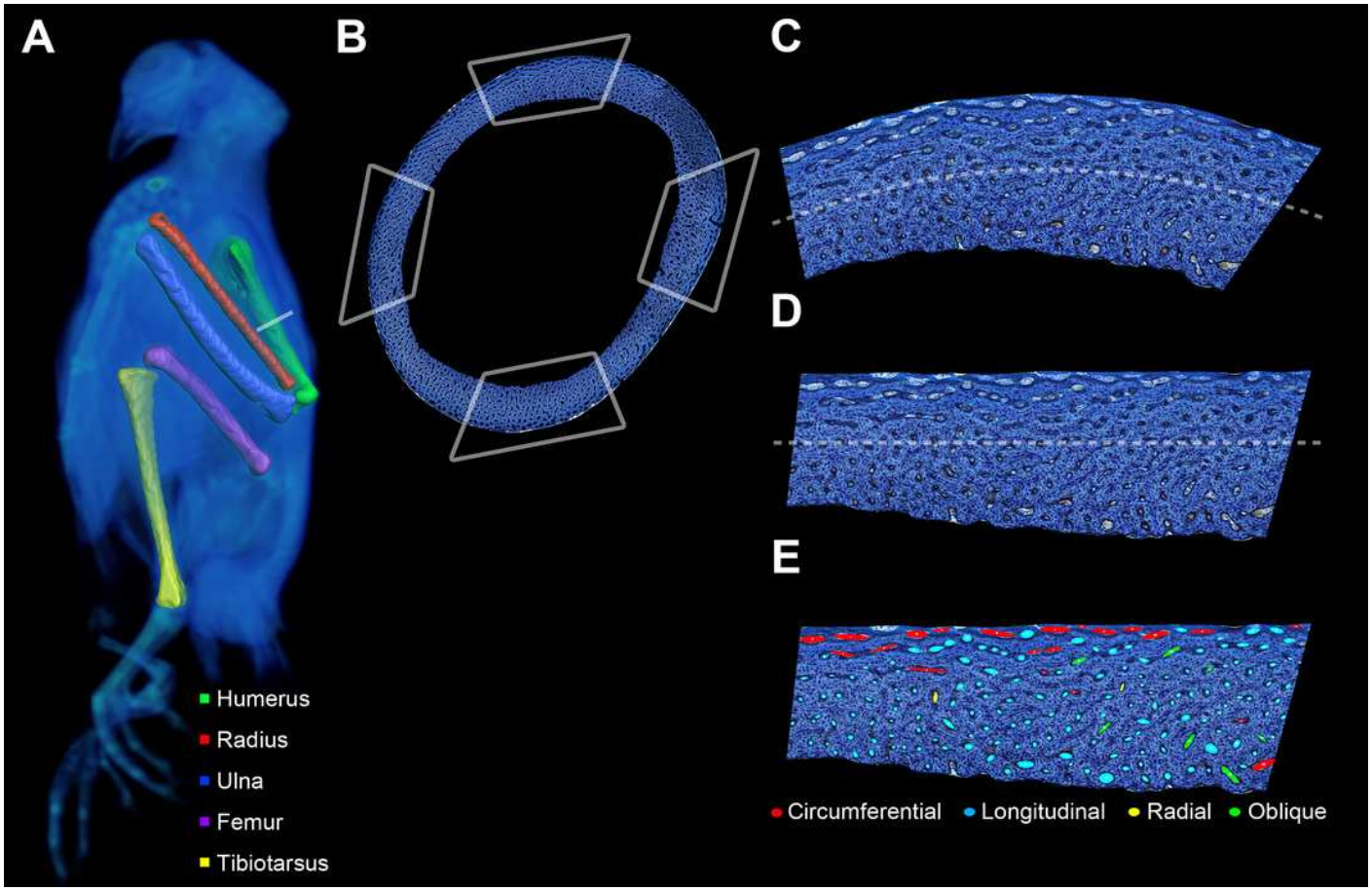

Figure 3

Histology of representative bone elements from growing pigeons arranged by mass.

In ascending order (bottom to top): 209 g (MWU 271), 242 g (MWU 258), 314 g (MWU 273), 455 g (MWU 256), and 482 g (MWU 254). Bone porosity decreases with mass. Circumferential vascular canals are most abundant in juvenile cortical bone from the humerus, ulna, and femur. Scale bar equals 600 µm (**A,B,D–F & K**), 480 µm (**G,L & M**), 400 µm (**I,J,N–P**), 343 µm (**Q,T–V**), and 300 µm (**C,H,R,S,W–Y**). Digital slides are available at http://paleohistology.appspot.com/Page/Columba_livia.html .

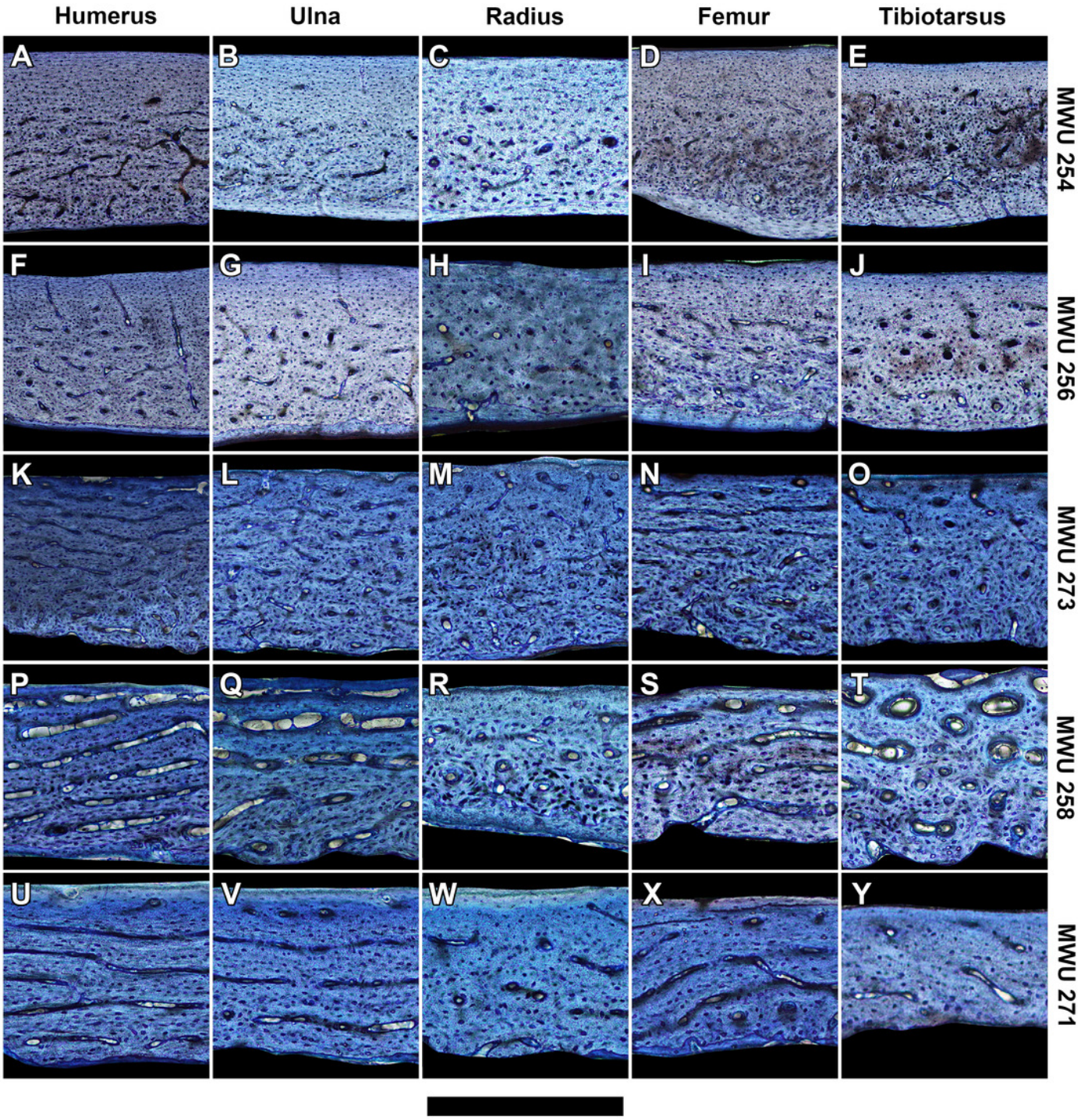
Humerus
Ulna
Radius
Femur
Tibiotarsus
A
B
C
D
E
F
G
H
I
J
K
L
M
N
O
P
Q
R
S
T
U
V
W
X
Y
MWU 254
MWU 256
MWU 273
MWU 258
MWU 271

Figure 4

Polar section modulus (Z_p) scaling analysis.

Positive allometric scaling of polar section modulus (Z_p) in humeri, ulnae, radii, femora, and tibiotarsi. Shaded regions are 95% confidence bands.

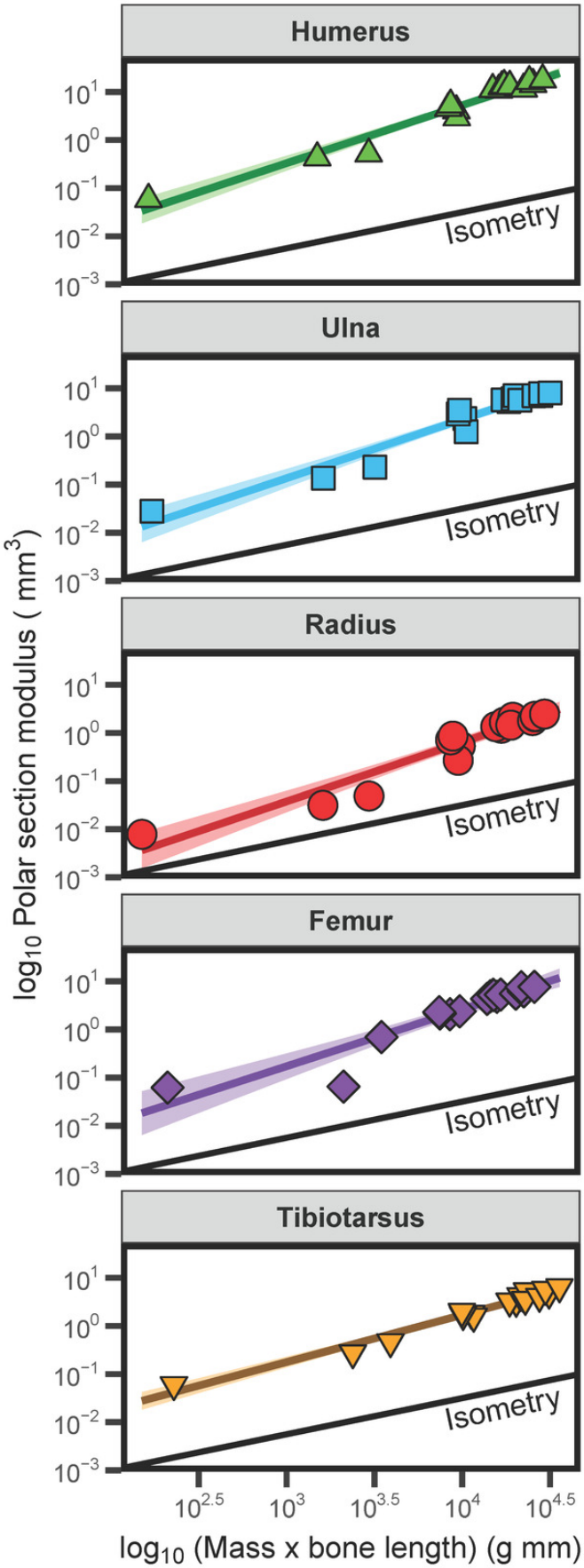
Humerus
Ulna
Radius
Femur
Tibiotarsus
Isometry
10^{1}
10^{0}
10^{-1}
10^{-2}
10^{-3}
$10^{2.5}$
10^{3}
$10^{3.5}$
10^{4}
$10^{4.5}$
$\log_{10}$ Polar section modulus (mm^3)
$\log_{10}$ (Mass x bone length) (g mm)

Figure 5

Relationship between laminarity and the "ontogenetic axis" of variation.

(**A**) humerus, (**B**) ulna, (**C**) radius, (**D**) femur, and (**E**) tibiotarsus.

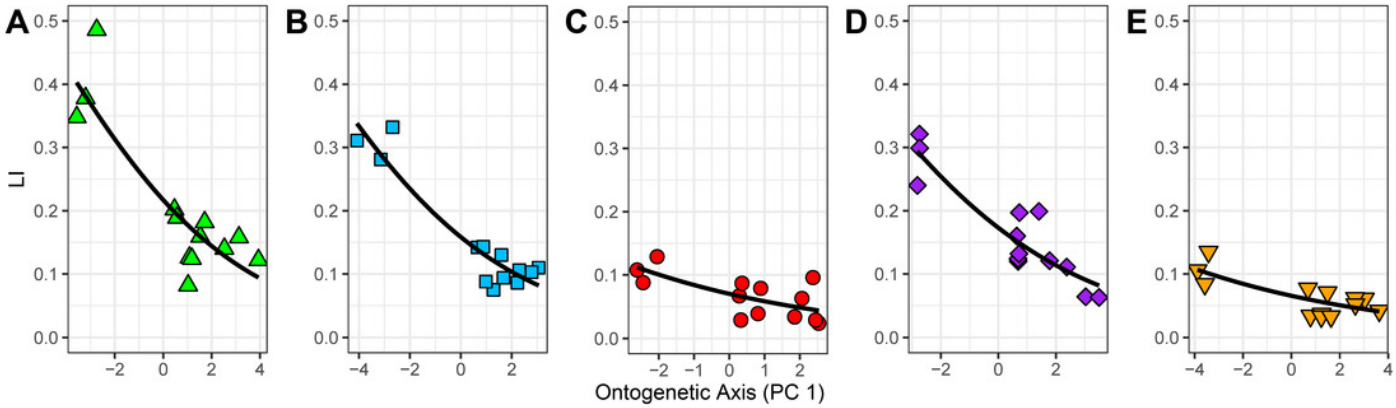

Table 1 (on next page)

Ontogenetic scaling of log10(midshaft polar section modulus of bone) and log10(body mass x bone length) .

Isometry equals slope of 0.75.

Table 1:
Ontogenetic scaling of log10(midshaft polar section modulus of bone) and log10(body mass x bone length).
Isometry equals slope of 0.75.

Element	Slope	95% CI	Intercept	95% CI
Humerus (*n* = 17)	1.20	1.07, 1.34	-4.09	-4.64, -3.54
Ulna (*n* = 17)	1.22	1.06, 1.39	-4.53	-5.20, -3.86
Radius (*n* = 17)	1.23	1.04, 1.43	-5.12	-5.90, -4.33
Femur (*n* = 17)	1.18	0.94, 1.43	-4.31	-5.28, -3.33
Tibiotarsus (*n* = 17)	0.98	0.89, 1.07	-3.69	-4.06, -3.31

Table 2 (on next page)

Results from robust principal component analysis (PCA).

Table 2:
Robust principal component analysis (PCA) results.

Element		PC1	PC2	PC3
Humerus	Eigenvalues	5.384	0.100	0.022
	Standard deviation	2.320	0.316	0.148
	Proportion of variance	0.978	0.018	0.004
	Mass eigenvector	0.262	-0.440	0.859
	Length eigenvector	0.522	0.813	0.258
	Z_p eigenvector	0.812	-0.381	-0.443
Ulna	Eigenvalues	5.581	0.115	0.048
	Standard deviation	2.362	0.339	0.218
	Proportion of variance	0.972	0.020	0.008
	Mass eigenvector	0.274	0.896	-0.350
	Length eigenvector	0.797	-0.415	-0.438
	Z_p eigenvector	0.538	0.159	0.828
Radius	Eigenvalues	3.184	0.168	0.018
	Standard deviation	1.784	0.409	0.133
	Proportion of variance	0.945	0.050	0.005
	Mass eigenvector	0.453	0.689	-0.566
	Length eigenvector	0.817	-0.575	-0.046
	Z_p eigenvector	0.357	0.441	0.823
Femur	Eigenvalues	3.963	0.047	0.038
	Standard deviation	1.991	0.217	0.196
	Proportion of variance	0.979	0.012	0.009
	Mass eigenvector	0.348	0.845	0.407
	Length eigenvector	0.689	-0.525	0.499
	Z_p eigenvector	0.635	0.107	-0.765
Tibiotarsus	Eigenvalues	6.706	0.233	0.048
	Standard deviation	2.290	0.483	0.218
	Proportion of variance	0.960	0.033	0.007
	Mass eigenvector	0.286	0.480	-0.830
	Length eigenvector	0.867	-0.499	0.010
	Z_p eigenvector	0.409	0.722	0.558

Table 3 (on next page)

Relationship between laminarity and principal components using beta regression

Standardized coefficients for each of the original variables (mass, Z_p, and bone length) are also listed.

Table 3:
Relationship between laminarity and principal components using beta regression.
Standardized coefficients for each of the original variables (mass, Z_p, and bone length) are also listed.

Element	Pseudo R^2	Intercept	p-value	PC1	p-value	Standardized Coefficients		
						Mass	Length	Z_p
Humerus	0.726	-1.283	9.47e-8	-0.249	1.22e-4	-0.065	-0.130	-0.202
Radius	0.440	-2.585	5.7e-10	-0.197	0.007	-0.089	-0.161	-0.070
Ulna	0.852	-1.670	2.0e-10	-0.245	2.29e-6	-0.067	-0.195	-0.131
Femur	0.819	-1.564	4.9e-10	-0.244	1.31e-5	-0.085	-0.168	-0.155
Tibiotarsus	0.521	-2.657	5.0e-11	-0.137	0.002	-0.039	-0.119	-0.056